Journal of Inorganic and Organometallic Polymers and Materials (2022) 32:1473–1486
https://doi.org/10.1007/s10904-021-02192-x

Development and Characterization of Antimicrobial Textiles from Chitosan-Based Compounds: Possible Biomaterials Against SARS-CoV-2 Viruses

María Florencia Favatela[1] · Jessica Otarola[1] · Victoria Belen Ayala-Peña[2] · Guillermina Dolcini[3] · Sandra Perez[3] · Andrés Torres Nicolini[4] · Vera Alejandra Alvarez[4] · Verónica Leticia Lassalle[1]

Received: 5 November 2021 / Accepted: 6 December 2021 / Published online: 28 January 2022

Abstract

Novel antiviral cotton fabrics impregnated with different formulations based on Chitosan (CH), citric acid (CA), and Copper (Cu) were developed. CA was selected as a CH crosslinker agent and Cu salts as enhancers of the polymer antimicrobial activity. The characterization of the polymeric-inorganic formulations was assessed by using atomic absorption spectroscopy, X-ray diffraction, Fourier transform infrared and UV–Vis spectroscopy, as well as thermogravimetric analysis. The achieved data revealed that CuO nanoparticles were formed by means of chitosan and citric acid in the reaction media. The antiviral activity of CH-based formulations against *bovine alphaherpesvirus* and *bovine betacoronavirus* was analyzed. Cotton fabrics were impregnated with the selected formulations and the antiviral properties of such textiles were examined before and after 5 to 10 washing cycles. *Herpes simplex virus type 1* was selected to analyze the antiviral activities of the functionalized cotton fabrics. The resulting impregnated textiles exhibited integrated properties of good adhesion without substantially modifying their appearance and antiviral efficacy (~ 100%), which enabling to serve as a scalable biocidal layer in protective equipment's by providing contact killing against pathogens. Thus, the results revealed a viable contribution to the design of functional-active materials based on a natural polymer such as chitosan. This proposal may be considered as a potential tool to inhibit the propagation and dissemination of enveloped viruses, including SARS-CoV-2.

Keywords Chitosan · Functional cotton fabric · Antiviral · Cu nanoparticles · SARS-CoV-2

✉ Victoria Belen Ayala-Peña
vayala@criba.edu.ar

María Florencia Favatela
florencia.favatela@outlook.es

Jessica Otarola
otarola_jessica@hotmail.com

Guillermina Dolcini
gdolcini@vet.unicen.edu.ar

Sandra Perez
seperez@vet.unicen.edu.ar

Andrés Torres Nicolini
andrestorresnicolini@gmail.com

Vera Alejandra Alvarez
alvarezvera@fi.mdp.edu.ar

Verónica Leticia Lassalle
velassalle@gmail.com

[1] Departamento de Química, INQUISUR, Universidad Nacional del Sur (UNS)-CONICET, 8000 Bahía Blanca, Argentina

[2] Departamento de Biología, Bioquímica y Farmacia, INIBIBB, Universidad Nacional del Sur (UNS)-CONICET, 8000 Bahía Blanca, Buenos Aires, Argentina

[3] Facultad de Ciencias Veterinarias, CIVETAN - CONICET, UNCPBA, 7000 Tandil, Argentina

[4] Facultad de Ingeniería, INTEMA, Universidad Nacional de Mar del Plata (UNMdP)-CONICET, 7600 Mar del Plata, Argentina

1 Introduction

In the last years, the use of bioactive molecules has attracted the attention of many researchers. Among them, Chitosan (CH) an interesting multipurpose, biodegradable, non-antigenic, non-toxic, and biocompatible natural polymer has gained huge popularity [1, 2]. This biopolymer is synthesized from chitin, which is one of the most abundant polysaccharides in natural macromolecules. Chitin is a typical component of mollusks, insect exoskeleton, fungal cell walls, and crustaceans, and it can be obtained from the waste of the latter [2]. Chitosan is not only a naturally renewable resource but also is a low-cost polymer and very versatile material. The availability of functional groups along its backbone makes it available for other polymers or metal ions to form bio-nano composites. Thus, it allows obtaining interesting derivatives [3], with numerous biological activities, such as antioxidant [4, 5], immunomodulatory [6], wound healing [7] and antitumoral [8, 9]. According to the available reports, bare CH has weak antimicrobial properties, which are not sufficient against certain groups of viruses and bacteria [10]. For this reason, the possibility of adding reinforcing agents or even performing its derivatization has been extensively studied [11–16]. Although less reported, CH and its derivatives are also well recognized as antiviral materials, Chirkov has cited several research findings to support the value of chitosan and various of its derivatives against viruses of different nature [17]. Nevertheless, as it was mentioned above, CH as a native molecule has limited activity as an antimicrobial agent over a wide range of viruses, but substitution at the amino group and hydroxyl group can significantly alter its efficacy against various viral strains [18]. In fact, different CH derivatives have been reported to have potential as anti-HIV agents [19–21]. Gao et al. have further demonstrated that 3, 6-O-sulfated chitosan was able to inhibit a broad spectrum of HPV pseudoviruses (HPV PV) [22]. Likewise, studies carried out by different authors highlighted the modified CH potential against influenza virus A [23]. Among CH derivatives, the presence of OH and NH_2 groups in this macromolecule favors its interactions with metals through the formation of stable chelate complexes. The bioactivity of some metallic moieties, i.e. from Ag, Cu, and Zn, are extensively known concerning their ability to inhibit several kinds of bacteria, fungi, and viruses [24, 25]. Between the two more useful metals, cooper is preferred because of its low cost, low toxicity, and bioavailability [26]. Thereby, the versatility associated with chitosan materials allowed its application in different areas; i.e. food industry as additives and in packaging preservation [27], chemical industry in the wastewater treatment [28], pharmaceutical industry as a drug carrier [29], biomedical industry in tissue engineering [30], agriculture [31] and in the textile industry [32]. This last application field has become a great challenge in view of the development of novel functional textile materials that have been accelerated in the pandemic context caused by SARS-CoV-2 during 2020 and presently. Due to the rapid and great mass mobilization of people across the planet, the emergence of the SARS-CoV-2 virus managed to be transmitted very effectively in the human population, bringing not only mortality but also psychological alterations to the surviving individuals [33, 34]. The current world pandemic situation demands smart antiviral/antimicrobial textiles for protective healthcare professionals and individuals able to be adapted to the new normality. The insertion of CH in the textile industry has been primarily in the form of fibers retaining the properties of the natural biopolymer in terms of reducing the growth of microorganisms, such as bacteria and fungi on cotton [35]. CH may also be used to give an antibacterial finish to different textile fibers through an impregnation process [36]. This last option is very attractive because of the simplicity of the procedure. However, the reported works related to textiles modified with chitosan focus their attention mainly on complex chitosan derivatives, increasing the cost of materials, the residues generation (some of them toxic), and complexing the procedure itself [37]. This manuscript deals with the preparation of different formulations based on CH crosslinked with citric acid (CA) as antiviral formulations to be incorporated in the process of fabrication of functional textiles. As it was commented, the properties of CH as an antimicrobial agent have been extensively reported. However, most of the available articles include complex derivatization of this polymer to assess the desirable properties [11, 12]. In this work, a novel insight is proposed by using the cross-linker agent (CA) and cooper salts as enhancers of the antiviral activity of CH-based formulations employing a very simplified methodology able to be implemented at industrial scale. CA, as well as, citrate-based biomaterials have become an important tool due to their biological characteristics, among which their antimicrobial power stands out [36]. Wen et al. have used citric acid as an effective enhancer to improve the mechanical and antibacterial properties of the synthesized chitosan-based films [37]. CA was selected considering its natural origin, low cost, and the aforementioned properties. Differents CH/CA/Cu ratios have been explored aiming to reach formulations with improved impregnation properties and differents antimicrobial responses to be adapted to textiles of diverse compositions. This focus further includes an exhaustive characterization to assess the physicochemical properties of the prepared materials, as well as to evaluate their potential as textiles functionalizers. Cotton fabric have been impregnated with selected

formulations, examining the efficiency of loading and the antiviral activity before and after between 5 and 10 washing cycles. The current contribution highlights and analyses the antiviral activities of chitosan-based formulations with regards to their potential to inactivate model viruses such as human *herpes simplex virus type 1* (HSV-1), *bovine alphaherpesvirus 1* (BoHV-1), and *bovine betacoronavirus* (BCoV). It is worth noting that viruses belonging to the *Herpesviridae family*, as well as those belonging to the *Coronaviridae family*, are classified within the group of enveloped viruses since in both families, viruses contain a superficial lipid membrane envelope with inserted proteins [38]. Therefore, the results obtained from the tests carried out on HSV-1, BoHV-1, and BCoV, which demonstrate an antiviral action of biopolymers against these viruses, are very promising to adduce how SARS-CoV-2 would respond to biopolymers. It is worth mentioning that SARS-CoV-2 studies deserve to be carried out. However, the biosecurity levels required for the use of this virus impose restrictions on these types of studies.

This contribution may be considered as a useful tool to the design of functional materials, especially textiles, with the potential ability to inhibit the SARS-CoV-2 and even other viruses dissemination, contributing to the reduction of virus spread and infection. The novelty of this research is given by the combination of raw materials and preparation methodologies that have not been before reported in open literature. Besides, from the application focus, this article provides improved alternatives to the design of antiviral textiles avoiding the wide spread use of bare metallic nanoparticles, the most commonly used compounds, that are actually questioned and limited, at least in Europe, because of possible leaching inducing possible toxicity. Functional textiles with biopolymeric based additives are not actually commercially available, to the best of the author´s knowledge, hence this investigation may contribute with valuable basic and potentially applicable data in the field of functional smart materials.

2 Experimental

2.1 Materials

All reagents used for the synthesis of the different chitosan-based formulations were of analytical grade and used without further purifications. Chitosan-powered (Aparent viscosity 16MPA.S; deacetylation degree 95.37%) was provided by Farmacia Homeopática Pereda (Mar del Plata, Argentina). The citric acid (99.8% purity) was from Anedra (Argentina) and copper sulfate pentahydrate ($CuSO_4$-$5H_2O$) (97% purity) was purchased from Cicarelli (Argentina). Distilled water was used for all the experiments.

2.2 Methods: Synthesis of Chitosan-Based Materials

2.2.1 CH.CA and CH.CA1

A 10 or 20% w/v citric acid (CH.CA or CH.CA1 respectively) aqueous solution was prepared. For this, the necessary volume of water was added to a weighed appropriate amount of citric acid under magnetic stirring at room temperature until dissolved all the acid. Then, the required amount of chitosan was added to the citric acid aqueous solution to obtain a final chitosan concentration of 8% w/v. The chitosan acid solution was kept under magnetic stirring for 1 h also at room temperature to achieve the complete dissolution of the biopolymer. The obtained formulation was a dark yellow viscous liquid and was stored at 4 °C prior to its characterization. Both formulations presented identical appearance (data not shown).

2.2.2 CH.CA 0.25% Cu, CH.CA 0.5% Cu.a, and CH.CA 0.5% Cu.b

Solutions of chitosan in citric acid were prepared following a similar procedure to the one described above (See 2.2.1.). A 5% or 10% w/v citric acid (CH.CA 0.25% and Cu, CH.CA 0.5% Cu.a or CH.CA 0.5% Cu.b, respectively) aqueous solution was prepared and the appropriated amount of chitosan was added to these acid solution to obtain a final chitosan concentration of 4 or 8% w/v (CH.CA 0.25% and Cu, CH.CA 0.5% Cu.a or CH.CA 0.5% Cu.b, respectively). Later, $CuSO_4$-$5H_2O$ solution was added to the same volume of the acid chitosan solution under stirring. Two different concentrations (0.25 and 0.5% w/v) of copper salt were used to obtain materials with different properties. The mixture was vigorously stirred for 30 s after the copper salt incorporation. The resultant formulations were maintained without stirring for 1 h. The entire procedure was carried out at room temperature and the obtained materials were kept at 4 °C before their characterization (Table 1).

2.3 Characterization

2.3.1 Atomic Absorption Spectroscopy (AAS)

Cooper content was measured by atomic absorption spectroscopy using GBC Avanta 932 equipment. CH.CA 0.25% Cu, CH.CA 0.5% Cu.a, and CH.CA 0.5% Cu.b samples were diluted in a solution of 10%HCl, sonicated to ensure a complete cooper release, and filtered with a 200 nm filter before the measurements. Also, the copper content in the washing waters of textiles impregnated with CH.CA 0.5% Cu.a, and

Table 1 Summary of the different CH:CA:Cu explored and the final appearance of the reached formulations

Formulation	CH (%w/v)	CA (%w/v)	CuSO4.5H2O (%w/v)	Physical appearance
CH.CA	8	10	–	Dark yellow viscous liquid
CH.CA1	8	20	–	Dark yellow viscous liquid
CH.CA 0.25% Cu	4	5	0.25	Moss-green material with a liquid consistency
CH.CA 0.5% Cu.a	4	5	0.5	Liquid light emerald green material
CH.CA 0.5% Cu.b	8	10	0.5	Moss-green liquid

CH.CA 0.5% Cu.b was determined after 5 and 10 washing cycles, following the same procedure.

2.3.2 X-Ray Diffraction (XRD)

X-ray diffraction data were collected using a PANalytical Empyrean 3 diffractometer with Ni-filtered, CuKα radiation, and a PIXcel3D detector. It was operated at a voltage of 45 kV and a current of 40 mA. The data were collected using a continuous scan mode with an angular speed of 2°/min for the angular range $5° \leq 2\Theta \leq 80°$.

2.3.3 Fourier Transformed Infrared Spectroscopy (FTIR)

The incorporation of copper into the chitosan-based materials was evaluated by Fourier Transform Spectroscopy, using a Thermo Scientific Nicolet iS50 in the frequency range of 400–4000 cm^{-1}. Before the measurements, samples were dried at room temperature and they were mixed with dry KBr powder and compacted.

2.3.4 UV–Vis Spectroscopy

Before the UV–Vis spectroscopy measurements, different mL of each material was diluted with distilled water. A spectrophotometer Shimadzu160 Japan was used to analyse CH, CH materials, and $CuSO_4$ aqueous solution.

2.3.5 Thermal Properties

Thermogravimetric measurements (TGA) of the synthesized materials were performed by using a TGA Q500 V20.13 Build 39 instrument. Tests were run from 30 to 800 °C at a heating rate of 10 °C/min under an N_2 atmosphere.

2.3.6 Transmission Electron Microscopy and Scanning Electronic Microscopy (TEM)

Microscopy (TEM, JEOL 100 CX II, Tokyo, Japan) was used to examine the morphology and estimate the size of CuO NPs in the CH matrix To this, analysis the samples were dispersed in ethanol, placed on 200 mesh Cu grids and dried at room temperature.

2.4 Antiviral Assays of the Chitosan-Based Materials

Antiviral activity was evaluated for *bovine alphaherpesvirus 1* (BoHV-1, Cooper strain) and *bovine coronavirus* (BCoV, Mebus strain), a *betacoronavirus*. Viral stock preparation and titration assays were performed in Madin–Darby bovine kidney cells (MDBK) and in human rectal adenocarcinoma cells (HRT-18), which are the adequate substrates for the replication of BoHV-1 and BCoV, respectively. Viral titers were determined by microplate titration using the method of Reed and Muench [39] and were expressed as $TCID_{50}$/mL (Tissue Culture Infectious Dose 50%/mL). The titers of the viral stocks were 10^7 $TCID_{50}$/mL for BoHV-1 and $10^{6.73}$ $TCID_{50}$/mL for BCoV and they were used at a concentration of 10^5–10^6 $TCID_{50}$/mL. For the preparation of the viral stock and BCoV titration, a culture medium without fetal bovine serum was used to which 0.05% trypsin was added. For the determination of the antiviral activity the following test was carried out in triplicate.

2.4.1 Binding Test

This test evaluates the ability of natural biopolymers to adsorb BCoV and BoHV-1 virions. The tests were carried out as Ciejka et al. [40] with minimal modifications.

2.4.1.1 Binding test with BCoV or BoHV-1 The polymers were evaluated undiluted (210 µL) and in dilutions (1: 3 to 1: 5 or from 10^{-1} to 10^{-3} for BCoV or BoHV-1 respectively). The dilutions were made in a culture medium (MEM/F12 or MEM for BCoV or BoHV-1 respectively) and then 40 µL of the virus was added to the previously mentioned concentration. Virus adsorption was carried out at room temperature with stirring for 30 min. After centrifugation at 16,000 g for 5 min, the supernatant was collected for viral isolation and titration. Titrations were carried out in HRT-18 or MDBK cells (for BCoV or BoHV-1 respectively).

2.5 Treatment of Cotton Fabrics

The selected cotton fabric for the experiment was Jersey doble Pesco-Tejido de punto. The cotton fabric was chosen considering its versatility of applications. These cotton fibers

were impregnated with the selected synthesized materials and their antiviral properties were examined before and after the washing cycles. The materials used in the process were selected based on the characterization and the results of the antiviral assays obtained in Sect. 2.4. The direct and easy industrial adaptation of the synthetic procedure was a criterion also applied to this selection.

2.5.1 Determination of Pick-up Percentage

For determination of the o pick-up percentage, 5 × 5 cm pieces of the selected textile were dried at 80 °C for 15 min. Then, they were weighed to obtain the weight of the dry textile (Wi). Subsequently, the pieces were washed in 100 mL of distilled water and contacted with 10 mL of the different CH-based formulations for 1 min. The material excess was removed from the textile with a wooden roller. The textiles were dried at 180 °C for 30 s. Afterward, they were completely dried at 40–45 °C and weighed again to obtain the weight of the textile after the impregnation test (Wf). With the weighing data, the mass increase after the impregnation of the different textiles with each chitosan material was calculated.

$$\%\text{Pick - up} = \text{Wf} - \text{Wi}/\text{Wf} \times 100$$

2.5.2 Washing Cycles

A glass reactor containing 100 mL of water was used to implement the washing cycles at room temperature. Samples were put in the reactor under magnetic stirring for 30 s. After five washes, the textiles pieces were left to dry in an oven at 40–45 °C for 30 min. Between each washing cycle, the water was refreshed in the vessel. The dry textiles were weighed to evaluate the pick-up percentage. The pick-up percentages after the washing cycles were obtained to compare with the pick-up percentage of the unwashed textile acquired in Sect. 2.5.1. and thus, to indirectly obtain the mass of formulation lost in the washings.

2.6 Antiviral Assays of the Functional Textile

2.6.1 Cell Cultures

Vero cells (African green monkey kidney) (ATCC, CCL-81) were grown in Dulbecco's Modified Eagle's medium (DMEM, GIBCO) supplemented with 5% fetal calf serum and were cultured at 37 °C in 95% air/5%CO_2 atmosphere. For maintenance medium (MM), the serum concentration was reduced to 1.5%.

2.6.2 Viruses Stock

Human *herpes simplex virus type 1* (HSV-1) strain Kos was propagated by infecting Vero cells. The cells were infected and incubated at 37 °C in an atmosphere containing 5% CO_2 until the monolayer showed almost 100% cytopathic effect (CPE), at about 2–3 days post-infection. CPE was evaluated using an inverted microscope. The samples were lysed by two freeze–thaw cycles and stored at − 80 °C. Samples from mock-infected cells were prepared and stored in the same manner. Virus yield was determined by virus titration on fully confluent cells seeded on 24 well plates, by plaque assay.

2.6.3 Viral Infection

Impregnated textiles were HSV-1 (10^3 PFU: plaque-forming unit) or mock-infected, 20 µL per cm^2, in simulated wet-droplet contamination, as described by Warnes and co-workers [41], and were incubated for different times at 25 °C. Then, 100 µL/of 2 M NaCl every 10^3 PFU was added to textiles as Ciejka [40]. The influence of 2 M NaCl on virus infectivity was evaluated. For this purpose, 20 µL of viral suspension was incubated at 25 °C throughout the experiment; finally, 80 µL of 2 M NaCl or PBS was added to the samples. Every sample was mixed for 15 min and then centrifuged for 1 min at 16,000 rpm. Subsequently, the virus was quantified in supernatants by plaque assay.

2.6.4 Plaque Assay

Vero cells were seeded into 24-well microplates and grown overnight. Tenfold dilution of supernatants was added to monolayers of confluent Vero cells at 37 °C for 1 h. Following incubation, the inoculum was removed, and monolayers were covered with 1 mL of DMEM containing 1% methylcellulose. The cells were incubated at 37 °C for 48–72 h and fixed using 4% formaldehyde. Finally, plaques were stained with 0.1% crystal violet in 20% ethanol and counted.

2.7 Statistical Analysis

GraphPad Prism software version 7 or 8 was used for statistical analysis. The results represent the average of at least three experiments, each condition ± SD unless otherwise indicated. Statistical significance was determined by ANOVA followed by Tukey's test with $p < 0.05$ considered significant.

3 Results and Discussion

3.1 Characterization of Different Chitosan-Based Formulations

The formulations achieved according to the combination of raw materials and conditions depicted in Table 1, exhibit differences related to the metal and CA content, which affects their physical aspect as well as their physicochemical properties. Figure 1 shows the physical appearance of the selected CH formulations including CA or Cu. As can be seen, materials with different appearances were obtained.

3.1.1 Atomic Absorption Spectroscopy (AAS)

The metal incorporation on the biopolymeric matrix was ascribed to provide improved antimicrobial properties as well as the better textile attachment. However, it is worth mentioning that a strict regulation exists regarding the inclusion of metallic moieties on textiles [42]. The limits and fastness values for copper in textiles for both uses, direct and non-direct contact with the skin, is 50 mg/kg of textile [43]. Despite this, the quantification of metals in impregnated textiles before and after wash cycles is not usually performed. To determine the real copper content in the CH.CA 0.25% Cu, CH.CA 0.5% Cu.a, and CH.CA 0.5% Cu.b formulations, AAS was used. The obtained results are presented in Table 2 together with the nominal copper content in each material.

Data in Table 2 show that the copper content obtained by AAS is in accordance with the expected values. It is important to highlight that pathogenic organisms such as viruses (including several coronaviruses, influenza virus, and HIV), bacterial strains, and fungi can be eliminated by copper after short periods of exposure [5]. The real copper content obtained in the different tested formulations is promising for the desired application compared to the copper values reported by different authors concerning antimicrobial materials design. For example, Imai et al. studied the antiviral effect of cotton textiles containing 0.5 g Cu^{2+}/m^2 of textile (CuZeo-textile) on a highly pathogenic H5N1 and low pathogenicity H5N3 viruses where they observed that the titers decreased by > 5.0 log10 after 30 s of incubation on the textile [6]. Horie et al. showed a reduction in the titer of the H9N2 virus by exposure to Cu^{2+} in concentrations of 2.5–250 µM [44]. Borkow et al. developed a mask impregnated with 2.2% w/w of copper oxide particles and tested its antiviral effects against influenza (H1N1 and H9N2) demonstrating that more than 99.85% of aerosolized viruses were filtered by the mask and no infectious influenza virus was found after 30 min [45]. This same author also used 2 mg/mL of powder copper oxide particles (of about 18 µm) to inactivate HIV in 5 min [46].

3.1.2 X-Ray Diffraction (XRD)

In Fig. 2, the wide X-ray diffraction patterns of the obtained CH-based formulations are compared. The goal was to investigate the influence of the crosslinking process with CA and the incorporation of metallic particles on the chitosan structure. CH is a semi-crystalline polysaccharide and exhibits two main reflection peaks at 2θ ~ 10° and 2θ ~ 20° [47]. The peak at 10° is assigned to the hydrated crystals due to the integration of water molecules in the crystal lattice, and the peak located at 20° is attributed to the regular crystal lattice of CH [48]. The diffractograms show a notable decrease in these two peaks, with the addition of citric acid. Formulations containing 10 and 20% w/v CA, lead

Table 2 Copper content of the different hydrogel formulations

	Nominal copper content (mg/g gel)	Copper content measured by AAS (mg/g gel)
CH.CA 0.25% Cu	10.89	9.33
CH.CA 0.5% Cu.a	20.90	16.91
CH.CA 0.5% Cu.b	10.88	8.58

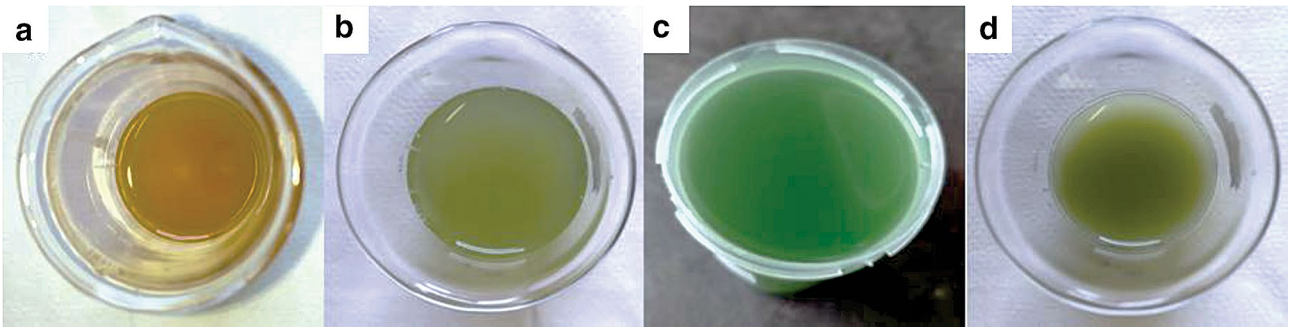

Fig. 1 Images of chitosan-based formulations. **a** CH.CA, **b** CH.CA 0.25% Cu, **c** CH.CA 0.5% Cu.a, and **d** CH.CA 0.5% Cu.b

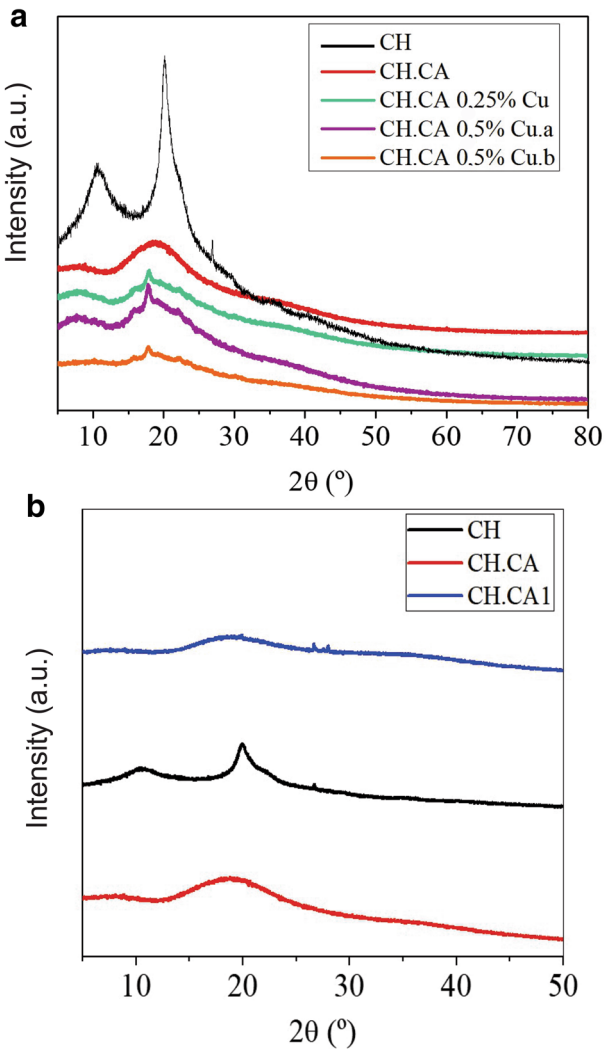

Fig. 2 X-ray diffraction patterns. **a** chitosan films of different formulations. **b** CH, CH.CA1, formulations

to non-crystalline diffraction peaks due to the interaction between CH and CA. It can be observed the broad scattering peak at 2θ of 20°, which is attributed to the amorphous halo of the molecules in the amorphous state [49]. Therefore; the observed pattern is compatible with amorphous films. These results are in agreement with those recently achieved by Zhuang et al. [50]. These authors have prepared CH-CA membranes by employing citric acid as the solubilizer and cross-linker. They found that interaction between citric acids and amino groups of chitosan can disrupt the crystalline structure in chitosan. Their XRD data confirmed the effect of CA in reducing the CH crystallinity. The diffraction peak at about 19.6° corresponding to the characteristic diffraction of crystallized chitosan without chemical modification became very broad, indicating a decrease of crystallinity. The figure, including the diffractograms achieved by these authors, shows strong similarities with the Fig. 2 of the present work. A clear decrease of the intensity of the peak intensity, as well as a shift of characteristic peaks towards lower angles, could be seen in the diffractograms of copper-containing formulations. This decrease in the ordered structure of the films is likely due to the modification of inter-and intra-hydrogen bonding [51].

The diffractograms of the different copper formulations shown in Fig. 2, display two main diffraction peaks at around 2θ = 19° and 23°, which are associated with the hydrated conformation of chitosan [52]. The absence of signals at angles of 36.40°,43.39°, 50.55°, and 74.08°, corresponding to the characteristic face-centered cubic (fcc) of copper lines indexed at (111), (111), (200) and (220), may be considered as indicative of the lack of bare Cu moieties in the CH-based formulations [53]. Similarly, signals ascribed to Cu oxides (CuO, Cu_2O) are not clearly detected. One hypothesis is that the angle where they should be seen overlaps with the broad peaks associated with the biopolymer [54]. Other authors have reached similar findings by synthesizing CH-Cu hydrogels. They reported that the XRD profiles of all samples showed characteristic diffraction peaks of CS (2θ = 20°), but none of them showed diffraction peaks of $Cu(OH)_2$ or any other Cu-based inorganic components. They further prepared a physical mixture between CH–Cu moieties containing similar proportions that the composite and the signals of the inorganic metal were detected in the XRD. Therefore, they concluded that the absence of Cu signals was not due to the detection limit of XRD because of the low amount of the inorganic element, they suggested that the Cu is compromised in interactions with CH affecting its crystalline identification [55].

3.1.3 Fourier Transformed Infrared Spectroscopy (FTIR)

Changes in the functionality of CH moieties may be detected by FTIR spectroscopy allowing to gain insight concerning the possible mechanism of formulation´s formation. In Fig. 3a, spectra of CH modified with two CA concentrations are included. Characteristic bands of both chitosan and citric acid are observed. The broad absorption band between 3600 and 3000 cm^{-1} is assigned to the stretching of –OH groups and –NH groups of the carbohydrate ring (black arrows) [43], the peaks at 1370 and 1309 cm^{-1} to –CH bending vibrations (white arrows), and the peak at 1069 cm^{-1} to the skeletal frequency of –C–O–C– (gray arrows) [42]. Also, a strong absorption peak at 1740 cm^{-1} was observed that was attributed to carboxyl groups of CA (yellow arrow) [42]. As it was extensively reported, Citric acid is known to form ionically cross-linked chitosan–citrate complex. Similar signals have been found by other researchers and were associated to the as mentioned complex. In particular, they found a C=O stretching band at around 1715 cm^{-1} corresponding to citric acid (red arrows) and a signal located at about 1380 cm^{-1}

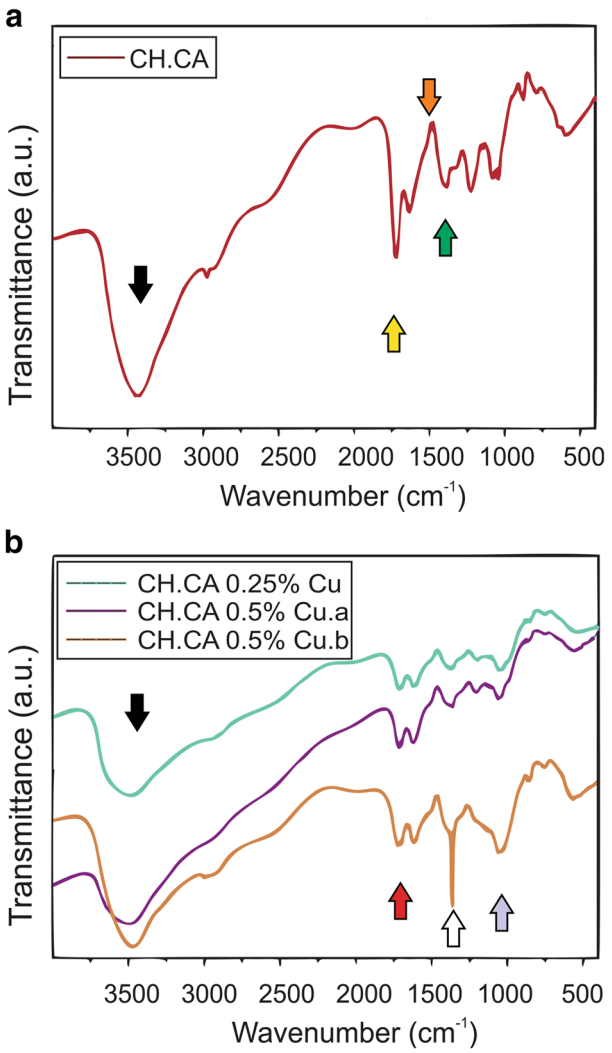

Fig. 3 FTIR spectra of **a** CH.CA and **b** CH.CA.Cu formulations

corresponding to the C–N of amide III in chitosan–citric acid membranes (green arrows) [50]. Besides, according with the reports in the literature, further bands assigned to ionically cross-linked CH-CA appear at around 1615 and 1512 cm^{-1}, which are mainly attributed to the antisymmetric $–NH^{3+}$ deformation and the symmetric $–NH^{3+}$ deformation (orange arrows), respectively, as suggested by Lawrie et al. [56]. These signals are slightly detected in the spectrum of Fig. 3a. In Fig. 3b, the bands described in Fig. 3a are observed, except for the one located at 1740 cm^{-1}, which shows lower intensity [43]. This may suggest the possible interaction between copper and carboxyl groups. In general, Cu moieties interact with chitosan due to its ability to chelate metals, through amine and hydroxyl groups. The ability of the biopolymer to act as a stabilizer promoting the formation of metallic nanoparticles has been reported [52]. Hence, Cu incorporation causes the shifts and variation of intensity in signal ascribed to OH and NH, mainly located between 3400 and 3600 cm^{-1} as observed in Fig. 3b. For instance, Jayaramudu et al determined that the in situ formation of CH-Cu NPs induced a shift and change in the CH characteristic peaks, especially the –OH and –NH stretching vibrations appeared at 3425 cm^{-1}. Then they assured that the registered shifting was majorly due to the formation and stabilization of Cu NPs [57]. In the particular case of the raw materials and methodology proposed within this work; and considering the lack of published information concerning the combination of CH-CA-Cu; it is possible to propose that the inter and intramolecular interactions between the CA and CH partially hinder the possibility to Cu to contribute to the crosslinking. Hence the level of metal-biopolymer interactions is low, determining that only a partial Cu NPs formation takes place. This fact represents an important difference with most of the published literature reports.

3.1.4 UV–Vis Spectroscopy

Figure 4 shows the obtained UV–Vis spectra of different formulations. The spectra of the materials formulated with copper show an absorption band between 270 and 300 nm that seems to be more intense with increasing metal concentration. These spectra were compared with the UV–Vis spectrum of a 1% solution of cupric sulfate, which presents an absorption peak at 810 nm attributed to Cu^{2+} ions in the solution [54]. This absorption peak was not found in the copper-containing formulations, suggesting that the copper in the formulations is as copper oxide nanoparticles. The region where the formulations exhibit absorption signals are compatible with the formation of cupric oxide nanoparticles (CuO) [58, 59]. The absorption region of bare Cu NPs as Cu_2O appears at 593 and 490 nm, respectively. Hence the occurrence of these Cu-based compounds may be discarded during the synthetic pathway involved within this work. These data are consistent with the development of colour observed during the preparation procedure (from the light blue of Cu^{2+} to brown-green CuO). These findings are consistent with reported researches [58]. The CH.CA formulation shows a slight absorption around 300 nm which is consistent with spectra of CH and CA reported by other authors [51].

3.1.5 TGA

The TGA curves of CH.CA, CH.CA 0.25% Cu, CH.CA 0.5% Cu.a and CH.CA 0.5% Cu.b are presented in Fig. 5a The TGA pattern of pure CH shows four characteristic step degradation patterns [60]. The first one around 100 °C, is related to water evaporation. The second degradation step, which determines the onset of structural degradation in CH, which represents the amine decomposition, reached a maximum at 395 °C. The third degradation step, which is

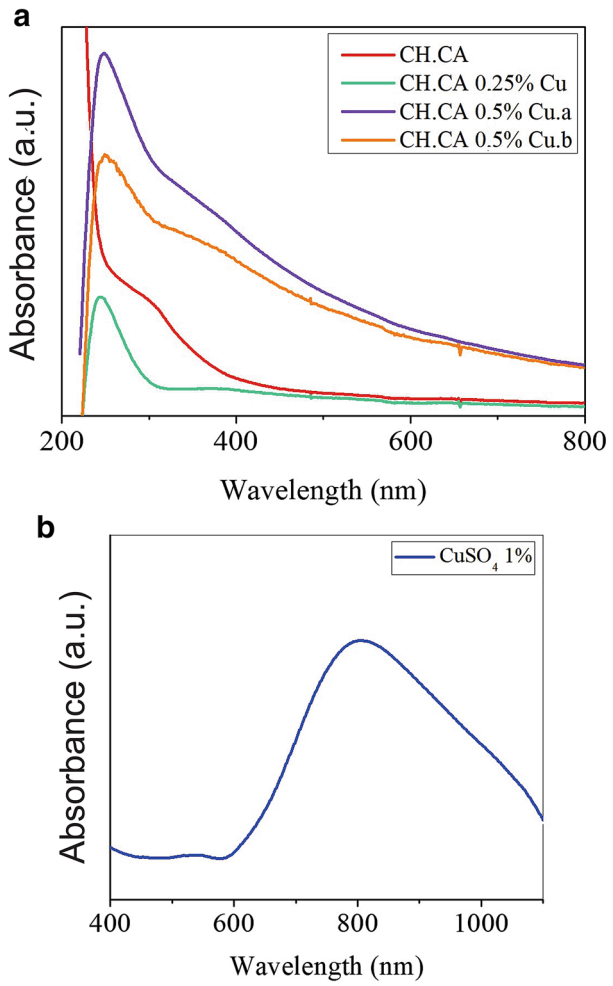

Fig. 4 UV–Vis spectra of **a** CH.CA, CH.CA 0.25% Cu, CH.CA 0.5% Cu.a, and CH.CA 0.5% Cu.b or **b** Sol $CuSO_4$ 1%

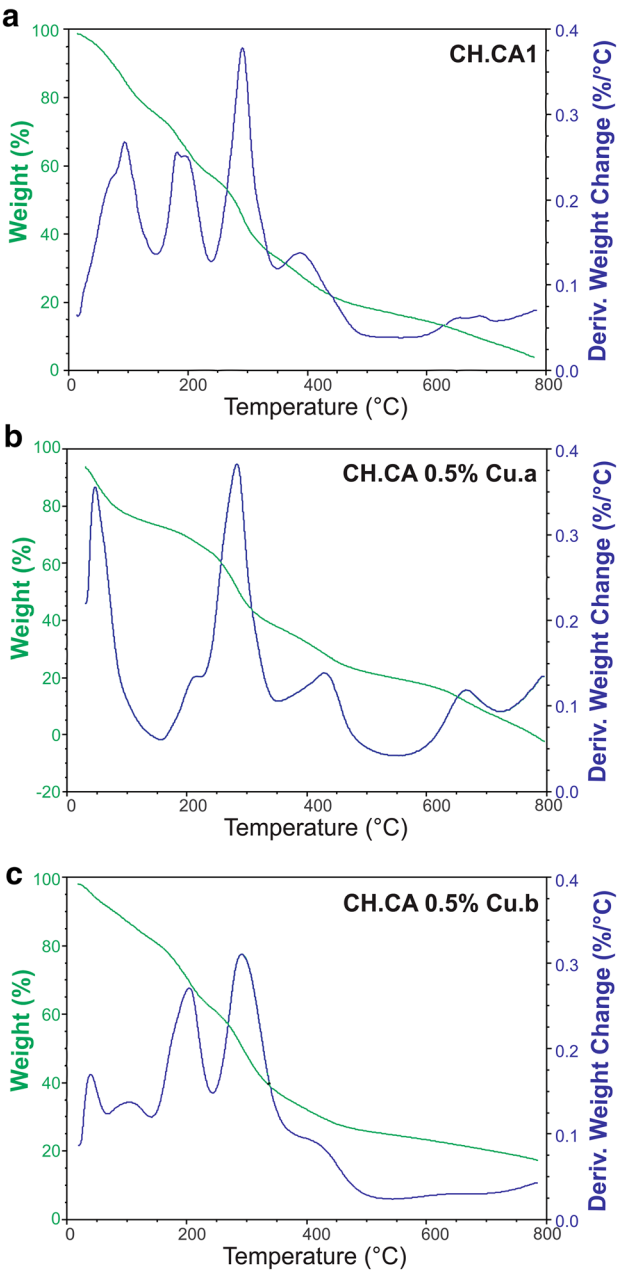

Fig. 5 TA and DTGA curves of: **a** CH.CA1, **b** CH.CA 0.5% Cu.a and **c** CH.CA 0.5% Cu.b

due to the decomposition of –CH2OH groups, went up to a maximum of 500 °C. The total degradation of the CH ring is responsible for the appearance of the fourth degradation step, corresponding to the degradation of cyclic ether present in the chitosan ring [61]. However, the degradation pattern of CH.CA (Fig. 5a) shows differences due to the citric acid. The first weight loss step related to the loss of water and other volatile material appears at 150 °C. In this case, there is a second weight-loss step around 225 °C and it is associated with the decomposition of CA [28]. The third weight loss step which corresponds to the amine degradation takes place at a relatively lower temperature (350 °C) than pure CH. And also, abrupt fourth step degradation around 550 °C is observed with a large weight loss within a small temperature window. This is presumed to be because of the breaking of cross-linked C–O–C bonds along with the cyclic C–O–C in the chitosan ring structure. The incorporation of different cooper concentrations does not lead to modifications in the thermal behavior, which is expected to give the thermal stability of these inorganic moieties.

The thermal stability of the formulations, once impregnated in the cotton fibers, was tested by promoting their heating in the range of temperatures usually employed in the textile industry in the different procedures that take place. In this case, they were between 80 and 180 °C and the textiles were demonstrated to be stable until 120 °C. These results, which were included in Supplementary Material, are in agreement with the ones corresponding to TG analysis.

3.1.6 TEM

In Fig. 6 the TEM micrographs of CH.Cu formulations are depicted. From the microscopic analysis, it is possible to distinguish the black spots associated with the inorganic nanoparticles dispersed in the polymeric matrix. As it was earlier commented the CH chains promoted the nucleus in formation stabilization rendered almost well dispersed nanoparticles. The presence of clusters of varied size is also observed leading to heterogeneous morphology. Similar findings have been reached in earlier works in the synthesis of magnetic nanoparticles stabilized by bulk chitosan. In such work, the co-precipitation of iron oxide nanoparticles was induced on the solid CH scaffolds that were dissolved in the ferric/ferrous. The resulted nanocomposites were characterized by a non-uniform distribution of magnetic nanoparticles stabilized by the polymeric moieties [62]. Hence from the TEM characterization allowed to verify the formation of the CuO NPs, in concordance with the UV–visible results.

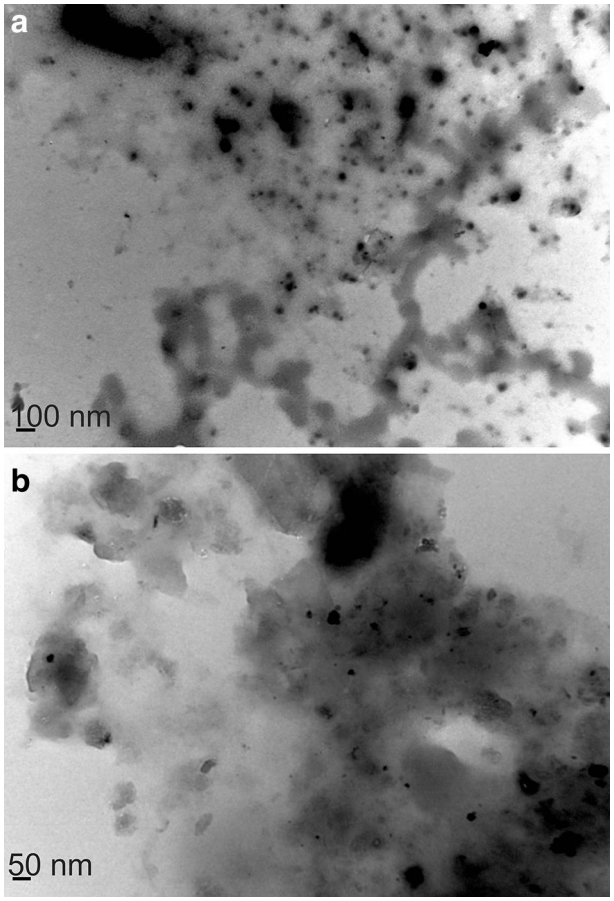

Fig. 6 TEM Micrographs of CH.Cu in **a** Magnification 100000x; **b** 50000x

3.1.7 Antiviral Assays of the Chitosan-Based Materials

The most suitable formulations in terms of their potential application on an industrial scale were analysed in terms of their antiviral capability. Specifically, CH.CA, CH.CA 0.5% Cu.a, and CH.CA 0.5% Cu.b formulations were selected to be analysed. Ciejka and co-workers demonstrated that CH formulations adsorbed several particles of coronavirus [40]. Viral activity was detected in none of the evaluated formulations, confirming 100% adsorption of BoHV-1. The average of the viral titers obtained for each formulation, with their corresponding dilutions, is represented in Fig. 7. Since CH.CA 0.5% Cu.a and CH.CA 0.5% Cu.b showed identical antiviral performance against BoHV-1, we decided to study the antiviral activity against BCoV with CH.CA and CH.CA 0.5% Cu.b. Figure 7b shows the results of the titrations carried out to determine viral titer after treatment with the two select biopolymers. As can be seen, undiluted CH.CA material adsorbed all of the viral particles without observing BCoV CPE after 72 h in culture. While in the case

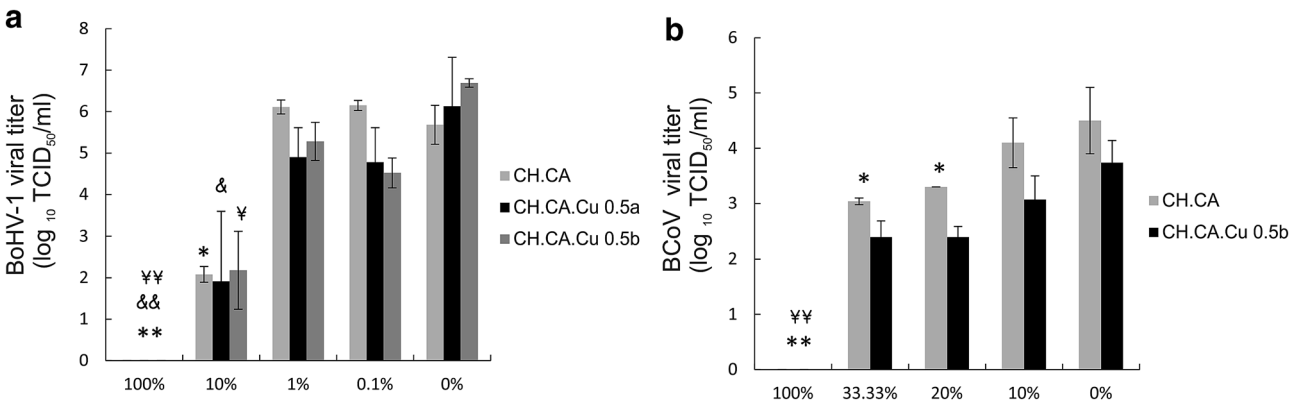

Fig. 7 **a** Results of viral titration after treatment of BoHV-1 (**a**) or BCoV (**b**) with different formulations. Values are expressed as means the SD from three experiments

of undiluted CH.CA 0.5% Cu.b formulation the viral titer obtained is minimum. When each CH formulations biopolymer was diluted in a 1: 3 ratio (33.33%), about mild viral CPE was detected, which was confirmed by direct immunofluorescence (data not shown). However, in the CH.CA 0.5% Cu.b (at 1:3 dilution) the viral titers achieved do not differ from what is observed when the formulation is used undiluted and are significantly lower ($p < 0.05$) than the titers detected for the control of BCoV in the absence of CH-based materials and those used in a lower concentration. This behaviour may be ascribed to the composition of the formulations, specifically to the interactions between these components and the viral particles. The capability of CH to inhibit bacteria and fungi is well known. Its antiviral properties, although less explored, have also been reported. The precise mechanism of its antiviral activity has not been well established. It is inferred that antiviral functionality relies on the direct interaction of the biopolymer with the viral particles, in particular with the S protein in the case of the coronaviruses enveloped viruses, such as those studied in this work. Hence it is assumed that the CH-virus interactions through S protein restrict the possibility of the viral particles entering the cell. Some authors have demonstrated that this biopolymer binds the recombinant ectodomain of the S protein, resulting in the formation of protein-polymer complexes. This binding leads to efficient inactivation of the virus [63, 64]. Besides, the high acidity content (CAC) strongly contributes to the observed antiviral response. Ayhan and Bilici informed that an acidic environment disrupts the cell wall structure causing a loss of ATP in the cell [65]. In addition, some authors reported that citric acid at a concentration of 1% effectively inactivated avian influenza virus (AIV) on hard and nonporous surfaces [66]. However, the incorporation of the Cu does not improve the capability of these formulations as antiviral with respect to CH.CA formulations at the conditions studied.

3.2 Textile Functionalization

The obtained pick-up% values can be seen in the following Table 3. The best impregnation of the textile was achieved with CH.CA, obtaining twice the % pick-up compared to the other materials. However, the data of pick-up after washings show a different trend. The incorporation of Cu strengthens the linkage between the formulation and the cotton. According to the available literature reports, long term interactions may be established by Cu incorporation. In particular, the CA and Cu combination appears as a determinant factor in the persistence of the formulation on the textiles. Furthermore, Roman and co-workers proposed that the bond of CuO and cotton is though OH-groups of cellulose (one of the main components of synthetic cotton), presumably by the formation of a complex-fiber bonding could have become a seed for the CuO NP [67].

Table 3 shows the pick-up percentage of the textile impregnated with the materials before and after being washed 5 and 10 times. The values of pick-up percentage were calculated as reported in Sect. 2.5.3. and show that there are no differences between the pick-up% obtained after 5 and 10 washes. Also, the procedure showed good reproducibility. To evaluate the loss of copper during the washings of the impregnated textiles, AAS was used. The textiles were washed following the methodology reported in Sect. 2.4.3. and the washing waters after 5 and 10 washes were collected. The results were presented in Table 4. As can be seen, there are no significant differences between the milligrams of copper leaching after 5 and 10 washes, respectively. Tamayo et al. report Cu^{2+} concentrations greater than 5 ppm released from chitosan-based copper nanocomposites immersed in an aqueous medium [68], while the data reported in this work, after 5 and 10 washes in an aqueous medium, demonstrated a release concentration of Cu^{2+} lower than 1 ppm. These values were favorable, since a higher concentration of Cu^{2+} remains in the textiles, prolonging their antiviral activity. Besides, the leaching of Cu found in these assays, assures safe materials in terms of the current textile regulation.

3.2.1 Antiviral Studies on Selected Functionalized Textile

For this study, we employed HSV-1, another enveloped virus, as SARS-CoV2. Both viruses belong to different families but they have a common lipid membrane that comes from infected human cells and superficial glycoproteins with tropism to human cell receptors. In an initial series of

Table 3 Pick-up % of the impregnation test for the different formulations

Sample	Pick-up (%)	Pick-up (%) after 5 washes	Pick-up (%) after 10 washes
CH.CA	19.70 ± 0.27	1.35 ± 0.47	1.05 ± 0.007
CH.CA 0.5% Cu.a	6.28 ± 0.31	2.28 ± 0.01	1.92 ± 0.00
CH.CA 0.5% Cu.b	10.75 ± 0.58	2.52 ± 0.29	2.18 ± 0.06

Table 4 Copper content in the washing waters of impregnated textiles

	Number of washes	Copper content measured by AAS	
CH.CA 0.5% Cu.a-impregnated textiles	5	0.57 mg	0.94 ppm
	10	0.57 mg	0.71 ppm
CH.CA 0.5% Cu.b-impregnated textiles	5	0.50 mg	0.83 ppm
	10	0.52 mg	0.65 ppm

experiments, HSV-1 was inoculated on CH.CA impregnated textiles (washed or not) for 2 min (Fig. 8). Approximately 10^3 PFU HSV-1 (20 µL) was applied to 1 cm^2 of CH.CA -impregnated and un-impregnated textiles and incubated at ambient conditions (21 °C; relative humidity, 30–40%). The virus was removed and assayed for infectivity at 2 min of exposition. Images of plaques were taken on day 2 post-infection in cell cultures. The results show a less % of virus titer reduction in washes conditions with respect to not washed CH.CA-impregnated textiles. These data provide the first evidence that HSV-1 can be inactivated by chitosan formulations. The following antiviral test was performed with CH.CA 0.5% Cu.b. Results revealed that the percentage of reduction of the viral titer of HSV-1 was almost 100 for impregnated textiles during the exposure time, while for untreated textiles the reduction was minimal (Table 5). The CH.CA 0.5% Cu.b- impregnated textiles with 10 washes maintained a lower antiviral activity at 1–2 min when compared with CH.CA 0.5% Cu.b- impregnated textiles without washes. However, the antiviral activity in the CH.CA 0.5% Cu.b- impregnated textiles with 10 washes reached the maximum at 30 min of exposure. The antiviral activity of CH.CA was so efficient and fast (100% inactivation in less than one minute) that copper failed to improve this score. However, copper managed to perpetuate the antiviral activity despite washing on textiles. These results suggest that the Cu incorporation improves the capability of these formulations as antiviral after washing concerning CH.CA formulation. Several studies demonstrated that chitosan can block viral attachment to host cells [40, 63]. However, the novel inactivation of HSV-1 with Chitosan has not been reported until now. A previous study demonstrated that a chitosan derivative shows anti coronavirus properties [40, 63]. Studies showed that the polymer interacts with the S protein of HCoV-NL63 and forms a protein-polymer complex, which results in virus neutralization [64]. A study demonstrated that *alphaherpesvirus* mutants deleted in several glycoproteins had lost the ability to be adsorbed to different proteins and peptides [65]. These studies suggest that the viral inactivation by chitosan could be through an unspecific interaction with viral glycoproteins evading the attachment to host cells. However, the HSV-1–chitosan-specific mechanism of inactivation should be studied. Modified textile showed antiviral activity against HSV-1, the viral titer was reduced by 100%, while untreated textiles cause no important decline in viral titers. Furthermore, we demonstrated here that the presence of Cu improves the persistence of antiviral activity despite the number of washes of the textiles respect CH.CA impregnated textiles. In addition, a large number of studies reported that coating materials containing metal ions (i.e., silver, copper, zinc), have an excellent antiviral ability with long-term, persistent effects [68–70].

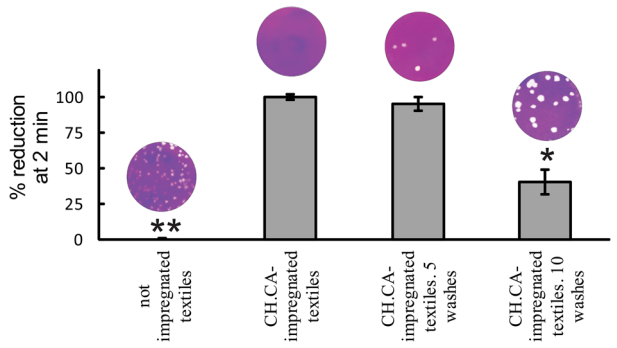

Fig. 8 Evaluation of HSV-1 virus titer in washed or not CH.CA-impregnated textiles at 2 min. Error bars represent ± SD, and data are from the results of three experiments

4 Conclusions

In the present work, antiviral textile materials were successfully obtained from the cotton treatment with novel CH-based formulations. The formation of CuO nanoparticles mediated by the biopolymers was evidenced based on the physicochemical characterization data. In this work, biopolymeric-based formulations demonstrated suitable properties to the textile impregnation as well as antiviral properties using BoHV-1 and BCoV, as models of the enveloped viruses. The antiviral properties of the functionalized textiles were examined before and after washing cycles. *Herpes simplex virus type 1* (HSV-1) was selected to analyse their antiviral activities. Modified textile showed antiviral activity against HSV-1. This work shows for the first time that these types of compounds have antiviral action on other viruses such as HSV-1 in addition to coronaviruses. The viral titer was reduced by 100%, while untreated textiles cause no important decline in viral titers. Also, it was demonstrated that the presence

Table 5 Evaluation of virus titers according to the exposure time in CH.CA 0.5%Cu.b-impregnated textiles

% Reduction	1 min	2 min	10 min	30 min
Not-impregnated textiles	2.1 ± 2.3	3.1 ± 1.3	14.0 ± 0.1	25.1 ± 0.50
CH.CA 0.5% Cu.b- impregnated textiles	100.1 ± 0.05	100 ± 0.05	100 ± 0.10	99.9 ± 0.50
CH.CA 0.5% Cu.b- impregnated textiles (5 washes)	99.2 ± 0.07	100.2 ± 1.1	100.2 ± 0.1	99.8 ± 0.08
CH.CA 0.5% Cu.b- impregnated textiles (10 washes)	89.0 ± 3.1	92.1 ± 2.2	98.1 ± 0.9	100.0 ± 0.2

of Cu improves the persistence of the antiviral activity independently of the number of washes of the textiles.

The selected CH-based formulation provided contact killing against pathogens. Thus, the results reveal a viable contribution to the design of functional-active materials proposing the use of chitosan as a potential molecule against SARS-CoV-2 viruses. These impregnated cotton fabrics can be used not only in medical applications but also for manufacture of textile products for daily use and technical textiles, such as for clothing in: the army, miners, medical care, sanitary masks, home fashion and household products, and sportswear. These new technologies are intended to meet the growing needs of the consumer in related antimicrobial textiles to safety, human health and the environment. Although now the focus is on the COVID-19 disease, the functional cotton proposed within this work may be efficient against other enveloped virus and even bacteria.

Supplementary Information The online version contains supplementary material available at https://doi.org/10.1007/s10904-021-02192-x.

Acknowledgements The authors thank to CONICET, FONARSEC (ANPCyT) Universidad Nacional del Sur and Universidad Nacional de Mar del Plata, Argentina.

Author Contributions MFF: investigation, methodology and formal analysis. JO: investigation, methodology and formal analysis. VBA-P: investigation, methodology and formal analysis and Writing—review & editing, GD: investigation, methodology and formal analysis, SP: investigation, methodology and formal analysis, ATN: methodology and formal analysis, VAA: Funding acquisition, project administration, resources, VLL: Funding acquisition, project administration, resources and Writing—review & editing.

Declarations

Conflict of interest There are no conflict to declare.

References

1. J. Yu, D. Wang, N. Geetha, K.M. Khawar, S. Jogaiah, M. Mujtaba, Carbohyd. Polym. **261**, 117904 (2021)
2. S.S. Vedula, G.D. Yadav, J. Indian Chem. Soc. **2**, 100017 (2021)
3. P.S. Bakshia, D. Selvakumar, K. Kadirvelu, N.S. Kumar, Int. J. Biol. Macromol. **150**, 1072–1083 (2020)
4. X. Li, S. Chen, J.E. Li, N. Wang, X. Liu, Q. An, X.M. Ye, Z.T. Zhao, M. Zhao, K.H. Ouyang, W.J. Wang, Cell. Longev. **21**, 1915967 (2019)
5. J.E. Li, W.J. Wang, G.D. Zheng, L.Y. Li, Int. J. Biol. Macromol. **95**, 719–724 (2017)
6. S. Zhang, H.L. Jiang, S.S. Huang, P.L. Li, F.S. Wang, Carbohydr. Polym **213**, 100–111 (2019)
7. L. Ling, X. Ronge, L. Jinguo, L. Pengcheng, Int. J. Polym. Mater. Polym. Biomater. **2020**, 1817017 (2020)
8. X.D. Dong, J. Yu, F.Q. Meng, Y.Y. Feng, H.Y. Ji, A. Liu, Cytotechnology **71**, 1095–1108 (2019)
9. G.N. Shi, C.N. Zhang, R. Xu, J.F. Niu, H.J. Song, X.Y. Zhang, W.W. Wang, Y.M. Wang, C. Li, X.Q. Wei, D.L. Kong, Biomaterials **113**, 191–202 (2017)
10. W. Wang, C. Xue, X. Mao, Int. J. Biol. Macromol. **164**, 4532–4546 (2020)
11. N.Y. Elmehbad, N.A. Mohamed, Int. J. Biol. Macromol. **151**, 92–103 (2020)
12. E.A.M. Azmy, H.E. Hashem, E.A. Mohamed, N.A. Negm, J. Mol. Liq. **284**, 748–754 (2019)
13. N.A. Mohamed, N.A. Abd El-Ghany, Int. J. Biol. Macromol. **115**, 651–662 (2018)
14. F.A. Alshubaily, Int. J. Biol. Macromol. **141**, 499–503 (2019)
15. A.M. Dias, M.P. dos Santos Cabrera, A.M.F. Lima, S.R. Taboga, P.S.L. Vilamaior, M.J. Tiera, V.A. de Oliveira Tiera, Carbohydr. Polym. **196**, 433–444 (2018)
16. S. Ejaz, A. Ihsan, T. Noor, S. Shabbir, M. Imran, Polym. Test. **91**, 106814 (2020)
17. S.N. Chirkov, Prikl. Biokhim. Mikrobiol. **5**, 13 (2002)
18. N. Sharma, C. Modak, P. Kumar Singh, R. Kumar, D. Khatri, S.B. Singh, Int. J. Biol. Macromol. **179**, 33–44 (2021)
19. M. Artan, F. Karadeniz, M.Z. Karagozlu, M.-M. Kim, S.-K. Kim, Carbohyd. Res. **345**, 656–662 (2010)
20. M.Z. Karagozlu, F. Karadeniz, S.-K. Kim, Int. J. Biol. Macromol. **66**, 260–266 (2014)
21. D. Wu, A. Ensinas, B. Verrier, C. Primard, A. Cuvillier, G. Champier et al., J. Mater. Chem. **4**, 5455–5463 (2016)
22. Y. Gao, W. Liu, W. Wang, X. Zhang, X. Zhao, Carbohydr. Polym. **198**, 329–338 (2018)
23. Y. Mori, T. Ono, Y. Miyahira, V.Q. Nguyen, T. Matsui, M. Ishihara, Nanoscale Res. Lett. **8**, 93 (2013)
24. S. Cheng, H. Zhao, Y. Xu, Y. Yang, X. Lv, P. Wu et al., Carbohydr. Polym. **107**, 132–137 (2014)
25. M. Zheng, D. Qu, H. Wang, Z. Sun, X. Liu, J. Chen et al., Sci. Rep. **6**, 28729 (2016)
26. L.L. Duffy, M.J. Osmond-McLeod, J. Judy, T. King, Food Control **92**, 293–300 (2018)
27. A. Manikandan, M. Sathiyabama, Nanomed. Nanotechnol. **6**, 1–5 (2015)
28. E. Kavitha, A. Sowmya, S. Prabhakar, P. Jain, R. Surya, M.P. Rajesh, Int. J. Biol. Macromol. **132**, 278–288 (2019)
29. M. Song, L. Li, Y. Zhang, K. Chen, H. Wang, R. Gong, React. Funct. Polym. **117**, 10–15 (2017)
30. P. Chen, L. Liu, J. Pan, J. Mei, C. Li, Y. Zheng, Mater. Sci. Eng. C **97**, 325–335 (2019)
31. M.G. Paulraj, S. Ignacimuthu, M.R. Gandhi, A. Shajahan, P. Ganesan, S.M. Packiam, N.A. Al-Dhabi, Int. J. Biol. Macromol. **104**, 1813–1819 (2017)
32. Y.L. Li, P.Y. Zhuang, Y.F. Zhang, Z.K. Wang, Q.L. Hu, Mater. Lett. **84**, 73–76 (2012)
33. J. Abbas, Psychiatr. Danub. **32**, 472–477 (2020)
34. J. Chen, Ch. Tian, X. Cheng, Y. Huang, L. Tang, R. Wang, X. Zeng, Psychiatr. Danub. **32**, 581–583 (2020)
35. M. Chuying, D. Gerhard, L. Di, Y. Yang, Biomaterials **178**, 383–400 (2018)
36. R.T. Tran, J. Yang, G.A. Ameer, Annu. Rev. Mater. Res. **45**, 277–310 (2015)
37. L. Wen, Y. Liang, Z. Lin, D. Xie, Z. Zheng, C. Xu, B. Lin, Polymer **230**, 124048 (2021)
38. G.P. Wormser, D.H. Rubin, *Fields—Virology (Two Volumes)*, 4th edn. (Lippincott Williams & Wilkins, Philadelphia, 2001)
39. L.J. Reed, H. Muench, Am. J. Hyg. **27**, 493–497 (1938)
40. J. Ciejka, K. Wolski, M. Nowakowska, K. Pyrc, K. Szczubiałka, Mater. Sci. Eng. **76**, 735–742 (2017)
41. S.L. Warnes, Z.R. Little, C.W. Keevil, MBio **6**, 01697–01715 (2015)

42. T. Abiraman, E. Ramanathan, G. Kavitha, R. Rengasamy, S. Balasubramanian, Ultrason. Sonochem. **34**, 781–791 (2017)
43. OEKO-TEX®-International Association for Research and Testing in Field of Textile and Leather Ecology. STADARD 100 by OEKO-TEX®. Edition 02/2020.
44. M. Horie, H. Ogawa, Y. Yoshida, K. Yamada, A. Hara, K. Ozawa, S. Matsuda, C. Mizota, M. Tani, Y. Yamamoto, M. Yamada, K. Nakamura, K. Imai, Arch. Virol. **153**, 1467–1472 (2008)
45. G. Borkow, S. Zhou, T. Page, J. Gabbay, PLoS ONE **25**, 5–6 (2010)
46. G. Borkow, C. Covington, B. Gautam, O. Anzala, J. Oyugi, M. Juma, M. Abdullah, Breastfeed Med. **4**, 165–170 (2011)
47. L. Leceta, M. Peñalba, P. Arana, P. Guerrero, K. de la Caba, Eur. Polym. J. **66**, 170–179 (2015)
48. L. Ren, X. Yan, J. Zhou, J. Tong, X. Su, Int. J. Biol. Macromol. **105**, 1636–1643 (2017)
49. J. Tanigawa, N. Miyoshi, K. Sakurai, J. Appl. Polym. Sci. **110**, 608–615 (2008)
50. L. Zhuang, X. Zhi, B. Du, S. Yuan, ACS Omega **5**, 1086–1097 (2020)
51. P. Guerrero, A. Muxika, I. Zarandona, K. de la Caba, Carbohyd. Polym. **206**, 820–826 (2019)
52. C. Qiao, X. Ma, X. Wang, L. Liu, LWT **135**, 109984 (2021)
53. M. Usman, N. Ibrahim, K. Shameli, N. Zainuddin, W. Md Zin, W. Yunus, Molecules **17**, 14928–14936 (2012)
54. A. Dehno Khalaji, K. Jafari, S. Maghsodlou Rad, J. Nanostruct. **4**, 14 (2012)
55. J. Nie, Z. Wang, Q. Hu, Sci Rep **25**(6), 36005 (2016)
56. G. Lawrie, I. Keen, B. Drew, A. Chandler-Temple, L. Rintoul, P. Fredericks, L. Grøndahl, Biomacromol **8**, 2533–2541 (2007)
57. T. Jayaramudu, K. Varaprasad, K. Koteshwara Reddy, R.D. Pyarasani, A. Akbari-Fakhrabadi, J. Amalraj, Int. J. Biol. Macromol. **145**, 825–832 (2020)
58. R. Sankar, P. Manikandan, V. Malarvizhi, T. Fathima, K.S. Shivashangari, V. Ravikumar, Spectrochim. Acta Part A **121**, 746–750 (2014)
59. G. Varughese, V. Rini, S.P. Suraj, K.T. Usha, Adv. Mater. Sci **42**, 49–60 (2014)
60. R. Priyadarshi, Y.S. Negi, J. Polym. Environ. **4**, 1087–1098 (2017)
61. R. Priyadarshi, B. Kumar, Y.S. Negi, Carbohydr. Polym. **195**, 329–338 (2018)
62. V. Lassalle, R. Zysler, M.L. Ferreira, Mater. Chem. Phys. **130**, 624–634 (2011)
63. A. Milewska, J. Ciejka, K. Kaminski, A. Karewicz, D. Bielska, S. Zeglen, W. Karolak, M. Nowakowska, J. Potempa, B. Jan Bosch, K. Pyrc, K. Szczubialka, Antivir. Res. **2**, 112–121 (2013)
64. A. Milewska, K. Kaminski, J. Ciejka, K. Kosowicz, S. Zeglen, J. Wojarski, M. Nowakowska, K. Szczubiałka, K. Pyrc, PLoS ONE **6**, 0156552 (2016)
65. B. Ayhan, S. Bilici, Turk. Hij. Den. Biyol. Derg. **4**, 323–336 (2015)
66. W. Chae, C. Cha, C. Yoo, S. Kim, H. Lee, J. Prev. Vet. Med. **42**, 16–21 (2018)
67. L.E. Román, M.J. Amézquita, C.L. Uribe, D.J. Maurtua, S.A. Costa, S.M. Costa, R. Keiski, J.L. Solís, M.M. Gómez, Adv. Nat. Sci. Nanosci. Nanotechnol. **11**, 025009 (2020)
68. J. Hodek, V. Zajicova, I. Lovetinska-Slamborova, I. Stibor, J. Muellerova, J. Weber, BMC Microbiol. (2016). https://doi.org/10.1186/s12866-016-0675-x
69. S. Miki, T. Ueda, D. Yamashina, K. Kinugawa, Coating agent composition and antibacterial/antiviral member. US Patent 10,131,797. 2018
70. G. Zeedan, K. El-Razik, A. Allam, A. Abdalhamed, H.A.A. Zeina, Adv. Anim. Vet. Sci. **8**, 433–443 (2020)